Results in Physics 6 (2016) 659–663

Contents lists available at ScienceDirect

Results in Physics

journal homepage: www.journals.elsevier.com/results-in-physics

Optimization of helical acquisition parameters to preserve uniformity of mouse whole body using multipinhole collimator in single-photon emission computed tomography

Naoyuki Ukon [a,b], Naoki Kubo [c,*], Masayori Ishikawa [d], Songji Zhao [e], Nagara Tamaki [f], Yuji Kuge [b]

[a] Department of Tracer Kinetics and Bioanalysis, Graduate School of Medicine, Hokkaido University, Japan
[b] Central Institute of Isotope Science, Hokkaido University, Japan
[c] Office of Health and Safety, Hokkaido University, Japan
[d] Department of Advanced Technology for Radiation Therapy, Graduate School of Health Science, Hokkaido University, Japan
[e] Advanced Clinical Research Center, Fukushima Global Medical Science Center, Fukushima Medical University, Japan
[f] Department of Nuclear Medicine, Graduate School of Medicine, Hokkaido University, Japan

ARTICLE INFO

Article history:
Received 26 August 2016
Received in revised form 12 September 2016
Accepted 15 September 2016
Available online 20 September 2016

Keywords:
Helical acquisition
Multipinhole collimator
Computed tomography
SPECT

ABSTRACT

Focusing on whole-body uniformity in small-animal single-photon emission computed tomography (SPECT), we examined the optimal helical acquisition parameters using five-pinhole collimators for mouse imaging. SPECT images of an 80-mm-long cylindrical phantom with ^{99m}Tc solution were acquired using an Inveon multimodality imaging platform. The bed travels used in this study were 0, 30, 60, 90 and 120 mm, and the numbers of revolutions traversed during the SPECT scan were 1.0, 2.0, 3.0, 4.0, 5.0 and 7.0, respectively. Artifacts that degrade uniformity in reconstructed images were conspicuous when the bed travel was smaller than the object length. Regarding the distal-to-center ratio (DCR) of SPECT values in the object's axial direction, the DCR nearest to the ideal ratio of 1.00 was 1.02 in the optimal uniformity with 4.0 revolutions and a bed travel of 120 mm. Moreover, the helical acquisition using these parameters suppressed the formation of artifacts. We proposed the optimal parameters in whole-body helical SPECT; the bed travel was sufficiently larger than the object length; the 4.0 or more revolutions were required for a pitch of approximately 30 mm/revolution. The optimal acquisition parameters in SPECT to preserve uniformity would contribute to the accurate quantification of whole-body biodistribution.

Introduction

Molecular imaging (MI) of small animals such as mice is a vital tool in basic scientific experiments and will provide important clues in pathology, physiology and pharmacology [1–4]. An exploratory investigational new drug study using MI can provide valuable information of a candidate drug concerning its pharmacokinetic properties and bioavailability, whole-body biodistribution and targeting properties [5]. Also, radiopharmaceutical research in animals has always been a vital step in the development of novel tracers and in the estimation of whole-body radiation exposure. Single-photon emission computed tomography (SPECT) imaging is particularly suited for pharmacokinetic analysis over a long term, because of the relatively long half-lives of γ-emitting radionuclides with in vivo kinetics. For small-animal SPECT, single-pinhole collimation is often used for high image magnification and high spatial resolution [6,7]. However, because of its low sensitivity, multipinhole such as five-pinhole SPECT with overlapping projections is also used to increase sensitivity over single-pinhole SPECT [8–12]. Overlapping pinhole projections or multiplexing and its resultant artifacts in reconstructed images are a concern [13–17]. Thus, sufficient sampling of acquisition is important to suppress multiplexing artifacts. Helical acquisitions using pinhole collimations can provide sufficient sampling data [7,18]. Also, axial bed motion can be used to acquire longer axial fields of view (FOVs), yielding whole-body biodistributions in SPECT systems with helical acquisition capabilities [19]. When the image uniformity of SPECT is improved, this will provide accurate quantitative information in small-animal studies [20]. In particular, a helical acquisition in SPECT to preserve whole-body

* Corresponding author at: Office of Health and Safety, Hokkaido University, Kita 8, Nishi 5, Kita-ku, Sapporo 060-0808, Japan. Fax: +81(11) 706 2295.
E-mail address: kubo-naoki@general.hokudai.ac.jp (N. Kubo).

http://dx.doi.org/10.1016/j.rinp.2016.09.010
2211-3797/

uniformity contributes to the accurate quantification of whole-body biodistribution. However, the optimal helical acquisition parameters for preserving whole-body uniformity using five-pinhole collimators have not been reported. In this paper, we focused on whole-body uniformity and we examined the optimal helical acquisition parameters in small-animal SPECT using five-pinhole collimators.

Materials and methods

SPECT experiments

The phantom used in this study was a cylinder made from acrylic with an inner diameter of 20 mm and a length of 80 mm, filled with a ^{99m}Tc solution with an activity of 740 MBq.

SPECT images were acquired using an Inveon multimodality imaging platform (Siemens Medical Solutions USA, Inc., Molecular Imaging, Knoxville, TN). The SPECT data were acquired over a period of 10 min and a sampling angle of 6° in the step-and-shoot mode. Five-pinhole tungsten collimators with 1.0 mm diameter pinholes (mouse whole body) were used at 40 mm from the center of the FOV. Three energy windows were set: a 20% photopeak window (126–154 keV), a lower window (112–126 keV) and an upper window (154–168 keV) for scatter correction. SPECT was carried out in the helical scan mode, with the axial bed motion while the dual head detectors are revolving. The bed travels used in this study were 0, 30, 60, 90 and 120 mm. The numbers of revolutions traversed during the SPECT scan were 1.0, 2.0, 3.0, 4.0, 5.0 and 7.0 corresponding to 120, 240, 360, 480, 600 and 840 total views in each bed travel, respectively.

A computed tomography (CT) image was acquired over approximately 10 min at 80 kVp and 500 μAs [21]. The CT image was used to acquire an attenuation map for attenuation correction of SPECT images [22].

SPECT data were reconstructed post hoc onto a 120 × 120 axial matrix with isotropic 0.5 mm voxels using a 3-dimensional ordered subset expectation maximization algorithm (zoom = 1; 30 iterations; 6 subsets) by incorporating scatter correction and CT-based attenuation correction [23]. SPECT data sets were visualized and analyzed using the Siemens Inveon Research Workplace 3D visualization software package (version 4.2) with no filter.

Data analysis

Multiplexing artifacts are observed in hot or cold regions as concentric rings in axial plane images [24]. We set nine rectangular solid regions of interest (ROIs; $2 \times 2 \times 10\ \mathrm{mm}^3$) concentrically, namely, one ROI at the distal part of the central axis in the cylindrical phantom (at 5 mm distance from the phantom bottom), four ROIs around and parallel to the earlier ROI (ROIs on the circumference of 4 mm radius), and four ROIs near the phantom periphery parallel to the earlier ROI (ROIs on the circumference of 8 mm radius). To evaluate artifacts that degrade uniformity as an artifact index (AI), an average normalized mean square error was applied:

$$\mathrm{AI} = \frac{1}{n}\sum_{j=1}^{n}\left(\frac{x_j - \bar{\lambda}}{\bar{\lambda}}\right)^2,$$

where n is the number of ROIs (=9), $\bar{\lambda}$ is the mean SPECT value of all ROIs, x_j is the SPECT value for individual ROIs and j is the ROI index [25]. When no artifacts occur, the artifact index is zero.

To investigate the effects of helical scanning on the phantom axial direction uniformity, two cylindrical ROIs (radius; 2.5 mm: height; 10 mm) were assigned at the distal part ($\mathrm{ROI_{distal}}$ at 5 mm distance from the phantom bottom in regions less affected by ring artifacts) and at the center ($\mathrm{ROI_{central}}$ at 35 mm distance from the phantom bottom in regions less affected by ring artifacts). The distal-to-center ratio (DCR) of the SPECT value in $\mathrm{ROI_{distal}}$ to that in $\mathrm{ROI_{central}}$ was evaluated. The DCR is higher than 1.00 if the SPECT values at the distal parts of the phantom are higher than that at the center. Also, the DCR is 1.00 if the uniformity is perfect.

To evaluate noise, $\mathrm{ROI_{central}}$ was evaluated on the basis of the coefficient of variation (COV), which is given by

$$\mathrm{COV}(\%) = 100 \times \frac{\sigma_v}{m_v},$$

where m_v is the mean SPECT value and σ_v is the standard deviation.

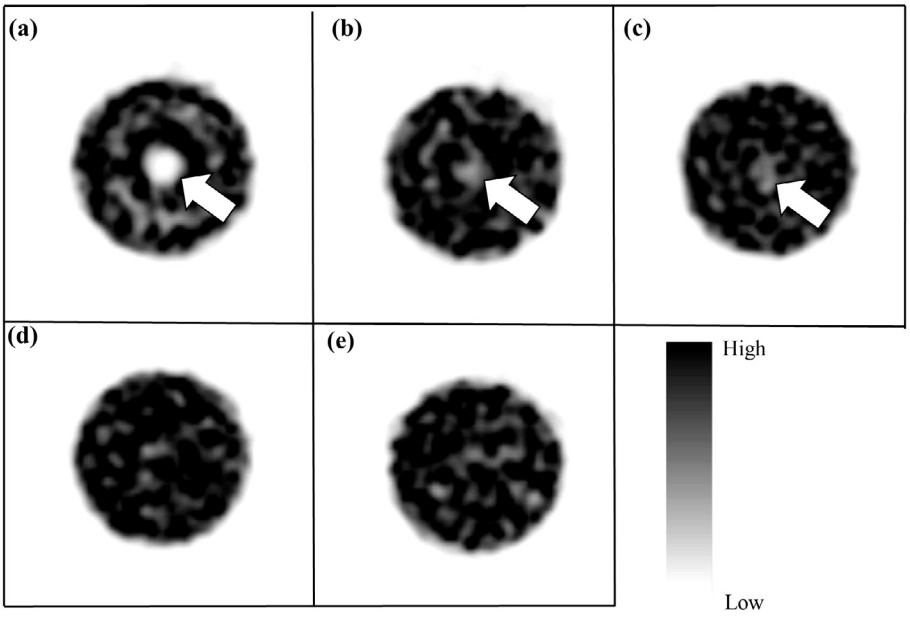

Fig. 1. For bed travels of (a) 0, (b) 30, (c) 60, (d) 90 and (e) 120 mm, reconstructed images of axial planes of the cylindrical phantom in helical SPECT scan are shown. The white arrows indicate remarkable artifacts.

Results

Fig. 1 shows axial images for observing easily the multiplexing artifacts with 5.0 revolutions. The multiplexing artifacts were observed as high- or low-intensity concentric regions in the short bed travel acquisitions. Particularly, the cold spots were found near the central axis in the short bed travel. On the other hand, these artifacts were suppressed when the bed travel increased to 90 mm and above.

Fig. 2 shows the dependence of the artifact index on the number of revolutions and the bed travel. At the bed travels of 0 and 30 mm, the artifact indexes were explicitly higher. When the bed travel was increased, the artifact index was decreased for all revolutions. To suppress multiplexing artifacts, bed travels equal to or greater than 90 mm are essential in this cylindrical phantom.

Fig. 3 shows coronal images for observing easily the effect of the number of revolutions with a bed travel of 120 mm. When the number of revolutions was 1.0, the image reconstruction was almost successful; however, the phantom shape at the center was visualized as somewhat narrow. For the numbers of revolutions ranging from 1.0 to 3.0, the SPECT values at the distal parts of the phantom were higher than that at the center. The image uniformity was improved by increasing the number of revolutions.

Fig. 4 shows the DCR as a function of the number of revolutions and bed travel. At a bed travel of 90 mm and above, the DCR nearest to the ratio of 1.00 was 1.02, with 4.0 revolutions and a bed travel of 120 mm. This parameter was equivalent to a pitch of 30 mm/revolution.

Fig. 5 shows the COV as a function of the number of revolutions for different bed travels. When the bed travel was increased, the COV was increased for all numbers of revolutions. Also, the COVs with 7.0 revolutions corresponding to 840 views were greater than those with other numbers of revolutions. At a bed travel of 120 mm, the COV with 4.0 revolutions was comparatively smaller than those with other numbers of revolutions.

Discussion

Focusing on whole-body uniformity, we examined the optimal helical acquisition parameters in small-animal Inveon SPECT using multipinhole collimators.

Using the 80-mm-long cylindrical phantom in this study, the bed travel of 120 mm and 4.0 revolutions corresponding to 480 views were the optimal measurement parameters because the arti-

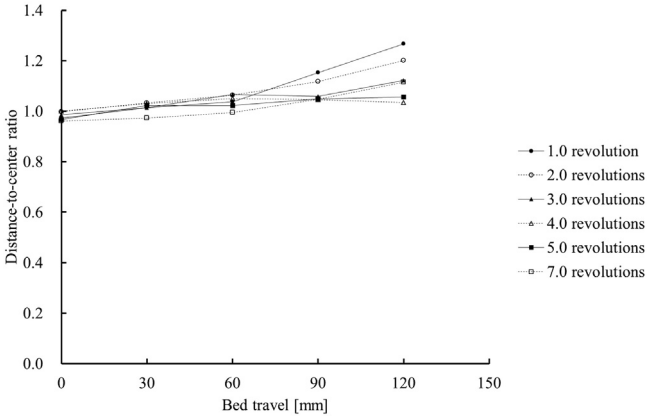

Fig. 4. Distal-to-center ratio (DCR) of cylindrical phantom as a function of bed travel and number of revolutions.

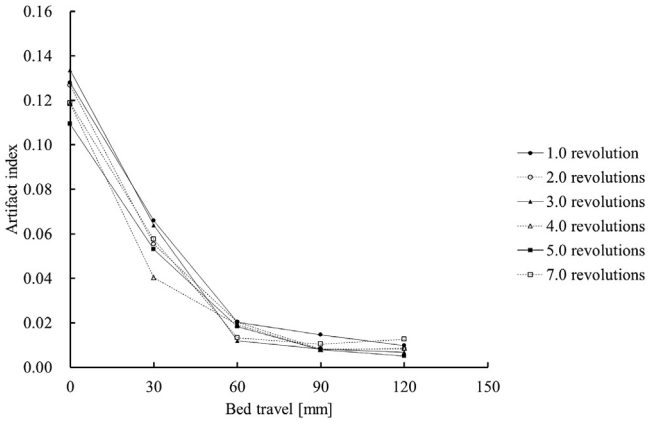

Fig. 2. Artifact index as a function of bed travel and number of revolutions.

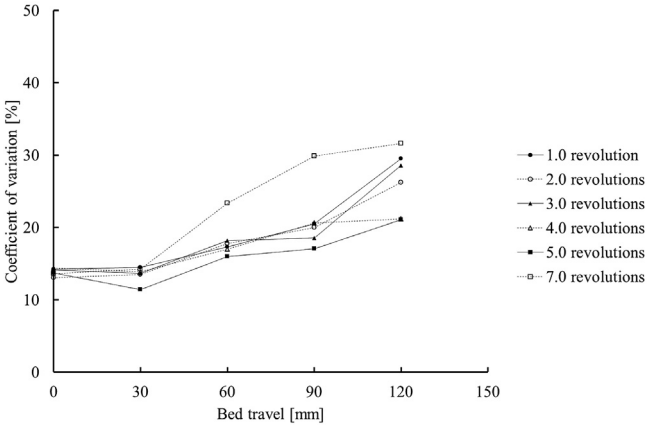

Fig. 5. Coefficient of variation (COV) as a function of bed travel and number of revolutions.

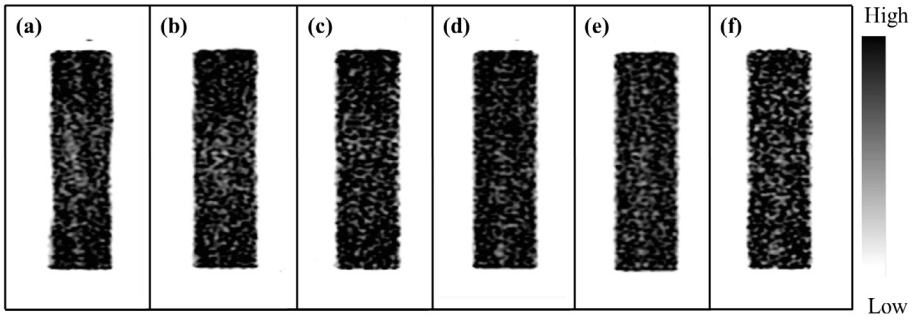

Fig. 3. For the number of revolutions of (a) 1.0, (b) 2.0, (c) 3.0, (d) 4.0, (e) 5.0 and (f) 7.0, the typical coronal slices of reconstructed images with a bed travel of 120 mm are shown.

fact index and COV were small and the DCR was near 1.00. These optimal parameters were equivalent to a pitch of 30 mm/revolution. Therefore, the optimal helical acquisition parameters in SPECT to preserve whole-body uniformity contribute to the accurate quantification of whole-body biodistribution for such an investigational new drug study.

If the bed travel is shorter, projection data of the distal edge of an object are not acquired. These cause truncation artifacts in the whole body [7]. Therefore, it is mandatory that the entire projection data are acquired to avoid missing the distal-edge projection data. By using a long bed travel and the distal-edge projection data with a blank space, we acquired non-overlapped projection data of the distal edge with five-pinhole collimators. Consequently, multiplexing artifacts could be suppressed by the non-overlapped projection data from multiple directions [15].

In the qualification of this study, the total acquisition time was constant for all bed travels and numbers of revolutions. The acquisition of blank spaces was an inefficient way of acquiring counts. Therefore, we did not conduct experiments with a bed travel of 150 mm.

It has been reported that an undersampling artifact could occur in pinhole SPECT, namely, insufficient sampling generates some artifacts [26]. Complete sampling is important in three-dimensional tomography and that is derived from the analysis of the data-missing domain in the Fourier space [27]. However, it may be difficult to analyze a reconstruction with multiplexing in the Fourier space. Consequently, it was useful that real experiments are performed for the evaluation of multiplexing artifacts.

In general tomography, projection data from multiple views are required [28]. In SPECT of multiplexing or overlapping projections, it is possible to reconstruct nearly true SPECT images when the SPECT scanner acquires many multiple views of different multiplexing. When the number of revolutions was increased, the number of views was increased in this study. Also, each view was different at the multiplexing of the object projection. Since many projection data from approximately five hundred views were acquired, it was possible to reconstruct nearly true phantom images. In this connection, these results were related to the geometry of five pinholes of Inveon. When the total acquisition time was constant and the number of views was increased, acquisition counts per 1 view decreased and the noise with 7.0 revolutions was increased in Fig. 5. Accordingly, too many projection data were unsuitable for image quality.

SPECT values at the distal parts of the phantom were higher than that at the center using insufficient sampling. These were SPECT value variations in the phantom axial direction or coronal planes. Therefore, these are related to the revolution and bed travel as the conditions in the object's axial direction. Sampling angle affects the image quality in axial planes. Even when a sampling angle was smaller than 6° used in this study, the multiplexing of the object's axial direction was almost unchanged. Thus, high SPECT values at the distal parts in the axial direction may not be affected by sampling angle.

In this study, the diameter of the phantom was 20 mm. The 20 mm diameter covers skeletons and internal organs of mice [29]. Also, another research group experimented with the 23-mm-diameter phantom for small-animal SPECT [30]. To image a larger object, a larger radius of rotation with degrading sensitivity is used. Nonetheless, we are experimenting with a large-size cylindrical phantom in a future study.

Spatial resolution was not considered in this research. However, these optimal helical acquisition parameters would lead to sufficient sampling and these should contribute to good spatial resolution.

Conclusion

In this paper, we propose the optimal helical acquisition parameters in small-animal whole-body SPECT using five-pinhole collimators. It is mandatory that projection data are acquired to avoid missing the distal-edge projection data in the object's axial direction. Thus, the bed travel is sufficiently larger than the object size. To acquire projection data from many multiple views such as nearly five hundred views, 4.0 or more revolutions were required for a pitch of approximately 30 mm/revolution. Consequently, the optimal helical acquisition parameters in SPECT to preserve uniformity will contribute to the accurate quantification of whole-body biodistribution for such an investigational new drug study or the estimation of whole-body radiation exposure.

Acknowledgements

This work was supported by Creation of Innovation Centers for Advanced Interdisciplinary Research Areas Program, Ministry of Education, Culture, Sports, Science and Technology-Japan and Innovative Medical Research based on quantum medical science and engineering.

References

[1] Acton PD, Kung HF. Small animal imaging with high resolution single photon emission tomography. Nucl Med Biol 2003;30:889–95.
[2] Loudos GK, Nikita KS, Giokaris ND, Styliaris E, Archimandritis SC, Varvarigou AD, et al. A 3D high-resolution gamma camera for radiopharmaceutical studies with small animals. Appl Radiat Isot 2003;58:501–8.
[3] Kubo N, Zhao S, Fujiki Y, Kinda A, Motomura N, Katoh C, et al. Evaluating performance of a pixel array semiconductor SPECT system for small animal imaging. Ann Nucl Med 2005;19:633–9.
[4] Gleason SS, Austin DW, Beach RS, Nutt R, Paulus MJ, Yan S. A new highly versatile multimodality small animal imaging platform. In: Nuclear science symposium conference record, 2006 IEEE. IEEE; 2006. p. 2447–9.
[5] Gomes CM, Abrunhosa AJ, Ramos P, Pauwels EKJ. Molecular imaging with SPECT as a tool for drug development. Adv Drug Delivery Rev 2011;63:547–54.
[6] Magota K, Kubo N, Kuge Y, Nishijima K, Zhao S, Tamaki N. Performance characterization of the Inveon preclinical small-animal PET/SPECT/CT system for multimodality imaging. Eur J Nucl Med Mol Imaging 2011;38:742–52.
[7] Metzler SD, Vemulapalli S, Jaszczak RJ, Akabani G, Chin BB. Feasibility of whole-body functional mouse imaging using helical pinhole SPECT. Mol Imaging Biol 2010;12:35–41.
[8] Feng B, Chen M, Bai B, Smith AM, Austin DW, Mintzer RA, et al. Modeling of the point spread function by numerical calculations in single-pinhole and multipinhole SPECT reconstruction. IEEE Trans Nucl Sci 2010;57:173–80.
[9] Lee S, Gregor J, Kennel SJ, Osborne DR, Wall J. GATE validation of standard dual energy corrections in small animal SPECT-CT. PLoS One 2015;10:e0122780.
[10] Osborne DR, Austin DW. Feasibility and initial performance of simultaneous SPECT-CT imaging using a commercial multi-modality preclinical imaging system. Int J Mol Imaging 2015;2015:1–11.
[11] Lee S, Gregor J, Osborne D. Development and validation of a complete GATE model of the Siemens Inveon trimodal imaging platform. Mol Imaging 2013;12:1–13.
[12] Boisson F, Zahra D, Parmar A, Gregoire MC, Meikle SR, Hamse H, et al. Imaging capabilities of the Inveon SPECT system using single-and multipinhole collimators. J Nucl Med 2013;54:1833–40.
[13] DiFilippo FP, Patel S. Strategies to reduce artifacts and improve accuracy in multiplexed multi-pinhole small animal SPECT. In: Nuclear science symposium conference record (NSS/MIC), 2009 IEEE. IEEE; 2009. p. 3151–4.
[14] Mok GS, Tsui BM, Beekman FJ. The effects of object activity distribution on multiplexing multi-pinhole SPECT. Phys Med Biol 2011;56:2635–50.
[15] Vunckx K, Suetens P, Nuyts J. Effect of overlapping projections on reconstruction image quality in multipinhole SPECT. IEEE Trans Med Imaging 2008;27:972–83.
[16] Mok GS, Wang YC, Tsui BM. Quantification of the multiplexing effects in multi-pinhole small animal SPECT: a simulation study. IEEE Trans Nucl Sci 2009;56:2636–43.
[17] Shokouhi S, Wilson DW, Metzler SD, Peterson TE. Evaluation of image reconstruction for mouse brain imaging with synthetic collimation from highly multiplexed SiliSPECT projections. Phys Med Biol 2010;55:5151–68.
[18] Metzler SD, Greer KL, Jaszczak RJ. Helical pinhole SPECT for small-animal imaging: a method for addressing sampling completeness. IEEE Trans Nucl Sci 2003;50:1575–83.
[19] Stout D, Berr SS, LeBlanc A, Kalen JD, Osborne D, Price J, et al. Guidance for methods descriptions used in preclinical imaging papers. Mol Imaging 2013;12:409–23.

[20] Aoi T, Zeniya T, Watabe H, Deloar HM, Matsuda T, Iida H. System design and development of a pinhole SPECT system for quantitative functional imaging of small animals. Ann Nucl Med 2006;20:245–51.
[21] Huang X, Wen D, Zhao W, Wang Q, Zhou W, Deng D. Skeleton-based tracing of curved fibers from 3D X-ray microtomographic imaging. Results Phys 2016;6:170–7.
[22] Marashdeh MW, Al-Hamarneh IF, Munem EMA, Tajuddin AA, Ariffin A, Al-Omari S. Determining the mass attenuation coefficient, effective atomic number, and electron density of raw wood and binderless particleboards of Rhizophora spp. by using Monte Carlo simulation. Results Phys 2015;5:228–34.
[23] Austin DW, Feng B, Mintzer R, Chen M, Gregor J, Stuckey AC, et al. Validation of CT-based attenuation correction for multi-pinhole PSF reconstruction for small-animal SPECT. In: Nuclear science symposium conference record (NSS/MIC), 2010 IEEE. IEEE; 2010. p. 3339–42.
[24] Lin JY. On artifact-free projection overlaps in multi-pinhole tomographic imaging. IEEE Trans Med Imaging 2013;32:2215–29.
[25] Johnson LC, Shokouhi S, Peterson TE. Reducing multiplexing artifacts in multi-pinhole SPECT with a stacked silicon-germanium system: a simulation study. IEEE Trans Med Imaging 2014;33:2342–51.
[26] Beque D, Nuyts J, Bormans G, Suetens P, Dupont P. Characterization of pinhole SPECT acquisition geometry. IEEE Trans Med Imaging 2003;22:599–612.
[27] Kudo H, Saito T. Feasible cone beam scanning methods for exact reconstruction in 3-dimensional tomography. J Opt Soc Am A 1990;7:2169–83.
[28] Zeng GL. Medical Image Reconstruction. Springer; 2010.
[29] Van Audenhaege K, Vanhove C, Vandenberghe S, Van Holen R. The evaluation of data completeness and image quality in multiplexing multi-pinhole SPECT. IEEE Trans Med Imaging 2015;34:474–86.
[30] Deleye S, Van Holen R, Verhaeghe J, Vandenberghe S, Stroobants S, Staelens S. Performance evaluation of small-animal multipinhole μSPECT scanners for mouse imaging. Eur J Nucl Med Mol Imaging 2013;40:744–58.